Journal of Materials Chemistry A

Nb-doped amorphous titanium oxide compact layer for formamidinium-based high efficiency perovskite solar cells by low-temperature fabrication

Journal:	*Journal of Materials Chemistry A*
Manuscript ID	TA-ART-03-2018-002540.R1
Article Type:	Paper
Date Submitted by the Author:	20-Apr-2018
Complete List of Authors:	Numata, Youhei; The University of Tokyo, RCAST Ishikawa, Ryo ; Saitama University, School of Engineering Department of Functional Materials Science; Ryo Ishikawa Sanehira, Yoshitaka; Toin University of Yokohama, Kogo, Atsushi; National Institute of Advanced Industrial Science and Technology, Shirai, Hajime; Saitama University Miyasaka, Tsutomu; Toin University of Yokohama, Graduate School of engineering

Journal Name

ARTICLE

Nb-doped amorphous titanium oxide compact layer for formamidinium-based high efficiency perovskite solar cells by low-temperature fabrication

Received 00th January 20xx,
Accepted 00th January 20xx

DOI: 10.1039/x0xx00000x

www.rsc.org/

Youhei Numata[a†]*, Ryo Ishikawa[b], Yoshitaka Sanehira[a], Atsushi Kogo[a‡], Hajime Shirai[b], and Tsutomu Miyasaka[a]*

Low-temperature processed perovskite solar cells (PSCs) were prepared with use of an amorphous niobium-doped titanium oxide (Nb/TiO_x) film as a compact layer (CL) combined with a brookite TiO_2 mesoporous layer. 4% Nb concentration in amorphous TiO_x CL was found to improve photocurrent-voltage performance of formamidinium (FA) and methylammonium (MA) mixed-perovskite, $(FAPbI_3)_{0.85}(MAPbBr_3)_{0.15}$, and $FA_{0.85}Cs_{0.15}PbI_3$ perovskite solar cells, which were fabricated on 100 °C and 130 °C-annealed TiO_x CL and yielded conversion efficiencies up to 19.1% and 19.8%, respectively. Nb/TiO_x-based $FA_{0.85}Cs_{0.15}PbI_3$ perovskite cell made entirely by low temperature process (130 °C or less) exhibited high stability against light soaking without encapsulation of device.

Introduction

Perovskite solar cells (PSCs) based on hybrid organic-inorganic lead halide materials have been attracting significant interest of researchers because of its high conversion efficiency, ease for fabrication in laboratory-scale, and potential of low cost production.[1-5] Since a conversion efficiency of 22.7% was achieved,[6] which is approaching a theoretical efficiency limit, importance of related technologies such as high device durability, low cost process, development of flexible device,[7-13] and lead-free materials[14-20] has significantly increased.

Low-temperature preparation of organic solar cells using metal oxide materials is a key technology to reduce process cost, and to fabricate tandem and flexible solar cells. The technology can reduce not only the process cost but also rise throughput in manufacture without using a time-consuming sintering and cooling processes. In fabrication of high efficiency tandem solar cells by using perovskite solar cells as a top cell of monolithic structure in combination with Si,[21-29] CuInGaSe (CIGS),[30-37] Cu_2ZnSnS_4 (CZTS),[38] and narrow band gap perovskite bottom cells,[39-43] preparation of top cell including metal oxide layers often requires low-temperature process to avoid thermal damage to lower layers and bottom cells. For same reason, invert structure type perovskite cells (employed in tandem top cells) requires low temperature for preparation of metal oxide top layers if they are used as electron collector or transparent conductors. Low process temperature is prerequisite to fabrication of flexible lightweight perovskite devices. In case of using plastic substrates, the most widely used polyethylene naphthalate (PEN) and polyethylene terephthalate (PET) films are stable less than 180 °C, and to avoid thermal shrinkage of the film, process temperature should be lower than 150 °C. In this aspect, we have so far developed methods of metal oxide preparation for PSC by using, for example, binder-free brookite TiO_2 nano-particles combined with low-temperature prepared SnO_2 and TiO_2 CLs.[10,44-47] Our method has enabled fabrication of flexible mesoscopic PSCs based on a plastic substrate with conversion efficiency up to 13.4%.[10] However, the conversion efficiency is still low, and thus, further development of low-temperature process is required. An issue in the low temperature metal oxide preparation is due to the amorphous property of the metal oxide CL, which requires precise adjustment of the thickness of considerably thin film (< 10 nm),[47] because of low conductivity and high carrier trap density. Carrier transport property of such crystalline and amorphous metal oxides can be controlled by doping of another metal ions such as indium tin oxide (ITO), NiO,[48,49] and ZnO.[50] Some heterometal-doped metal oxides were reported as n-type or p-type semiconductors for carrier transporting layers in PSCs such as Li-doped TiO_2,[51,52] Zn-doped TiO_2,[53] Y-doped TiO_2,[54] Nb-doped TiO_2,[55-58] Na-treated TiO_2,[59] K-doped TiO_2,[60] Sm-doped TiO_2,[61] Li-doped SnO_2,[62] Nb-doped SnO_2,[63] Y-doped SnO_2,[64] Li-doped ZnO,[50] La-doped $BaSnO_3$,[65] $NiMgLiO_x$,[58] $NiMgO_x$,[66] and

[a] Graduate School of Engineering, Toin University of Yokohama, 1614 Kurogane-cho, Aoba-ku, Yokohama, Kanagawa, 225-8503 Japan. *Email - y_numata@dsc.rcast.u-tokyo.ac.jp
[b] Department of Functional Materials Science, Graduate School of Science and Engineering, Saitama University, Sakura-ku, Saitama, 338-8570 Japan.
† Present affiliation, Research Center for Advanced Science and Technology (RCAST), The University of Tokyo, e-mail: y_numata@dsc.rcast.u-tokyo.ac.jp.
‡ Present affiliation, National Institute of Advanced Industrial Science and Technology (AIST).

Electronic Supplementary Information (ESI) available: [SEM images and optical properties of Nb-doped TiO_x films. All photovoltaic data of FA-MA PSC and FA-Cs PSC; optimization of Nb-doping ratio, thickness, and annealing conditions for CL and perovskite films]. See DOI: 10.1039/x0xx00000x

Cs:NiO_x.[67] For the challenge, we focused on an amorphous Nb-doped titanium oxide as an appropriate candidate of the low-temperature prepared CLs. Hasegawa et al accurately studied a crystalline Nb-doped TiO_2 (c-Nb/TiO_2) as a promising alternative of transparent conducting oxide (TCO) materials.[68-70] Nb(V) ion has comparable ionic radii (0.064 nm) with Ti(IV) ion (0.061 nm), and can easily form solid solution with TiO_2.[71] Nb ion behaves as an n-type dopant of TiO_2 and significantly enhance electron conductivity. PSCs using Nb-doped TiO_2 CLs sintered above 500 °C were reported.[55,57] Liu and Liu et al also reported Nb-doped titanium oxide as CL in planar-type PSCs and achieved more than 19% conversion efficiency.[56] They prepared the CL by dipping method and the CL was sintered at 185 °C; however, it is still higher than appropriate temperature for our target. Han et al firstly reported an amorphous Nb/TiO_x film as a hole-blocking layer in an inverted type PSC.[58] In the PSC, the Nb/TiO_x film was casted on electron extracting PCBM layer and dried at 70 °C. By Nb-doping, resistivity of the amorphous TiO_x film was significantly decreased, and resulting conversion efficiency was improved.

In this report, we newly prepared an amorphous niobium-doped titanium oxide (Nb/TiO_x) film as a compact layer of mesoscopic perovskite solar cells at dry temperature of 100 and 130 °C for two different perovskites, which are same with the annealing temperature of the corresponding perovskite layers. In our strategy of process design, condition of "low-temperature" should be the temperature range that is no higher (or less) than the temperatures employed for perovskite preparation and annealing. As perovskite layers, we prepared dual cation-halide perovskites, $(FAPbI_3)_{0.85}(MAPbBr_3)_{0.15}$ and $FA_{0.85}Cs_{0.15}PbI_3$ which exhibit high stability against heat and durable efficiency.

Results and discussion

Characterization of Nb-doped TiO_x compact layer

We prepared TiO_x films without and with Nb ion (doping ratio: 1, 2, 3, 4, and 5%) as a CL of PSCs. To clarify the result, only non-doped and the most Nb ion doped (5%) CLs were characterized and compared by XRD and XPS measurements. At first, we observed surface SEM images of the TiO_x CLs dried at 100 °C and sintered at 500 °C as shown in Figure S1. For the amorphous TiO_x CL dried at 100 °C, its surface seemed to be smooth and top and edge of FTO surface textures became fuzzy. We cannot observe any pinholes and cracks on the top and bottom of the FTO crystals. In contrast, at the surface of high temperature sintered CL, small crystal grains appeared and shape of FTO grains are sharp. Such granular particles possess grain boundaries and such sharp FTO crystal edges are exposed bare FTO surface, meaning electronic pinholes.

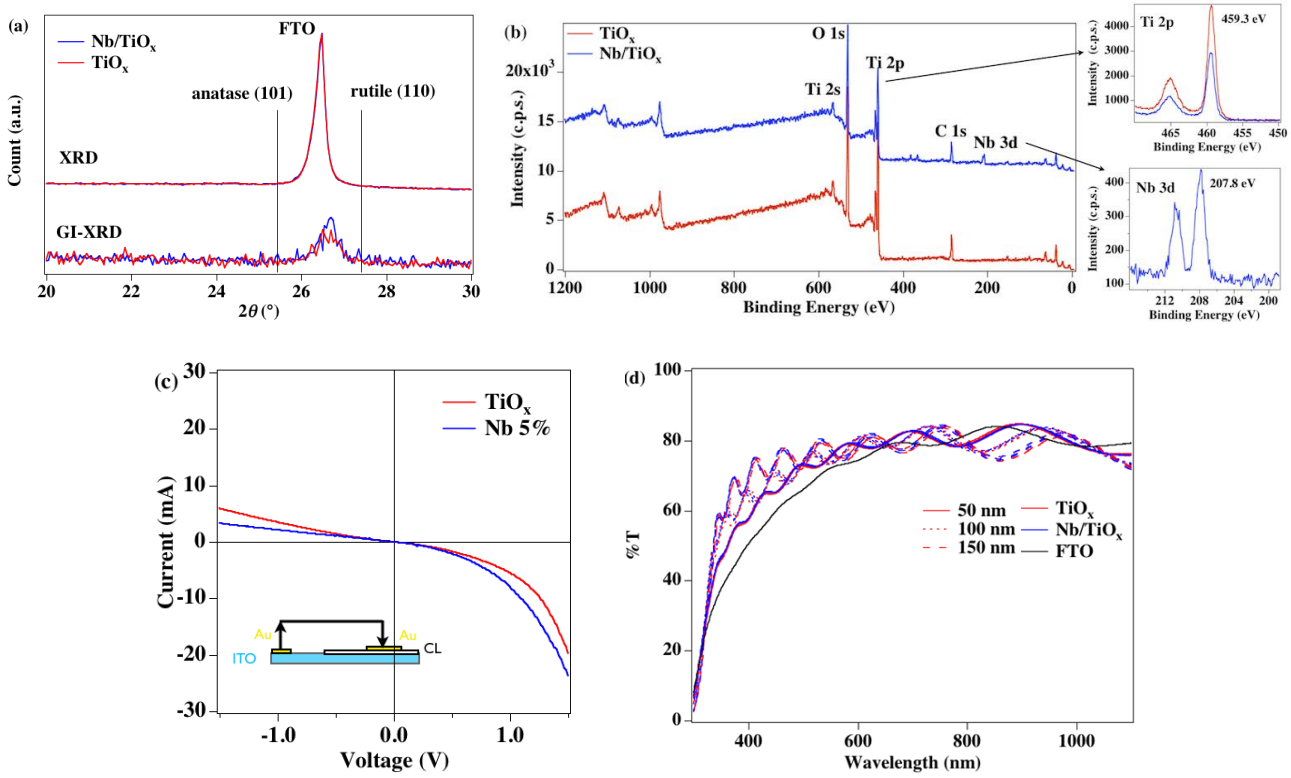

Figure 1. (a) Normal and GI-XRD diffraction chart of TiO_x and (5%) Nb/TiO_x CLs dried at 100 °C on the FTO substrate. (b) XPS spectra of TiO_x and (5%) Nb/TiO_x CLs on the FTO substrate dried at 100 °C. (c) *I-V* curves of ITO/CL (< 10 nm)/Au device dried at 100 °C for Nb-doped TiOx. inset: schematic illustration of the measured device. (d) Transmittance of TiO_x and (5%) Nb/TiO_x CLs on FTO substrates with different thicknesses dried at 100 °C.

Then, the obtained CLs were characterized by grazing incident (GI)-XRD measurement. Figure 1a shows normal and GI-XRD pattern of (5%) Nb/TiO_x and TiO_X films (film thickness > 100 nm) dried at 100 °C on a FTO substrate. For both films, diffraction peaks corresponding to anatase (101) and rutile (110) TiO_2 at 2θ = 25.4 and 27.4°, respectively, were not observed, indicating amorphous metal oxide films.

We confirmed existences of Nb atom in a TiO_x film by XPS spectroscopic measurement. Figure 1b shows XPS spectra of TiO_x and (5%) Nb/TiO_x CL films dried at 100°C (in Figure S2, XPS spectra of 150 °C dried films). Both films showed characteristic peaks assigned to Ti and O atoms from TiO_X. A peak position of Ti 2p orbital is observed at similar position of 459.3 eV for both CL films, which is matched with that of Ti(IV) of TiO_2 at 458.5 eV. Only in the Nb/TiO_x film, Nb 3d peak appeared at 207.5 eV, which is matched with Nb(V) of Nb_2O_5. Therefore, based on XRD and XPS results, we concluded that Ti and Nb atoms in the CL film are retained as fully oxidized state but not crystallized.

Figure 1c shows *I-V* curves of ITO/CL/Au sample (sample configuration is shown inset) to evaluate series resistivity of the CLs for TiO_X and 5% Nb-doped TiO_X on ITO substrate dried at 100 °C. Film thickness of the CLs are less than 10 nm. By Nb-doping, resistance of the TiO_x CL was decreased; however, there was no significant difference for the films because of very thin CL thicknesses.

Next, we observed film properties of the CLs by *I-V* and transmittance measurements. Figure 1d shows transmittances of the TiO_x and (5%) Nb/TiO_x CLs on a FTO substrate dried at 100 °C with the thicknesses of 50, 100, and 150 nm, respectively (transmittances of 130 and 150 °C dried films are

Table 1. Photovoltaic parameters of $(FAPbI_3)_{0.85}(MAPbBr_3)_{0.15}$-based PSCs with or w/o different Nb doped CLs dried at 100 °C.

Compact layer	scan direction[a)]	J_{SC} (mA cm^{-2})	V_{OC} (V)	*FF*	η (%)	No. of cells
TiO_x	forward	21.08±0.91 (20.51)	1.12±0.01 (1.14)	0.48±0.10 (0.63)	11.3±2.3 (14.7)	17
	reverse	19.86±0.62 (19.60)	1.15±0.01 (1.16)	0.73±0.06 (0.78)	16.6±1.2 (17.8)	
Nb 1%	forward	21.08±1.32 (23.01)	1.06±0.02 (1.06)	0.51±0.07 (0.62)	11.5±2.2 (15.0)	13
	reverse	20.99±0.84 (22.46)	1.12±0.01 (1.12)	0.73±0.03 (0.74)	17.1±1.0 (18.7)	
Nb 2%	forward	21.52±0.46 (21.89)	1.10±0.02 (1.13)	0.51±0.10 (0.66)	12.1±2.7 (16.3)	22
	reverse	21.10±0.66 (21.90)	1.14±0.01 (1.16)	0.73±0.04 (0.78)	17.5±1.0 (19.1)	
Nb 3%	forward	21.74±0.64 (22.17)	1.11±0.02 (1.12)	0.53±0.05 (0.62)	12.9±1.3 (15.4)	14
	reverse	20.89±1.30 (21.43)	1.14±0.02 (1.15)	0.72±0.04 (0.75)	17.0±1.2 (18.6)	
Nb 4%	forward	21.75±0.67 (22.26)	1.12±0.02 (1.15)	0.57±0.06 (0.65)	13.9±1.7 (16.5)	26
	reverse	21.15±0.75 (21.98)	1.15±0.01 (1.15)	0.75±0.01 (0.76)	18.2±0.7 (19.1)	
Nb 5%	forward	20.57±1.08 (21.39)	1.09±0.01 (1.11)	0.41±0.08 (0.55)	9.3±2.3 (13.1)	12
	reverse	19.69±1.43 (20.62)	1.12±0.01 (1.13)	0.70±0.05 (0.75)	15.5±2.1 (17.6)	

[a)] scan direction: forward $J_{SC} \rightarrow V_{OC}$ and reverse: $V_{OC} \rightarrow J_{SC}$. In parentheses, the parameters of the best cell. Cell active area is 5 × 5 mm² defined by black mask.

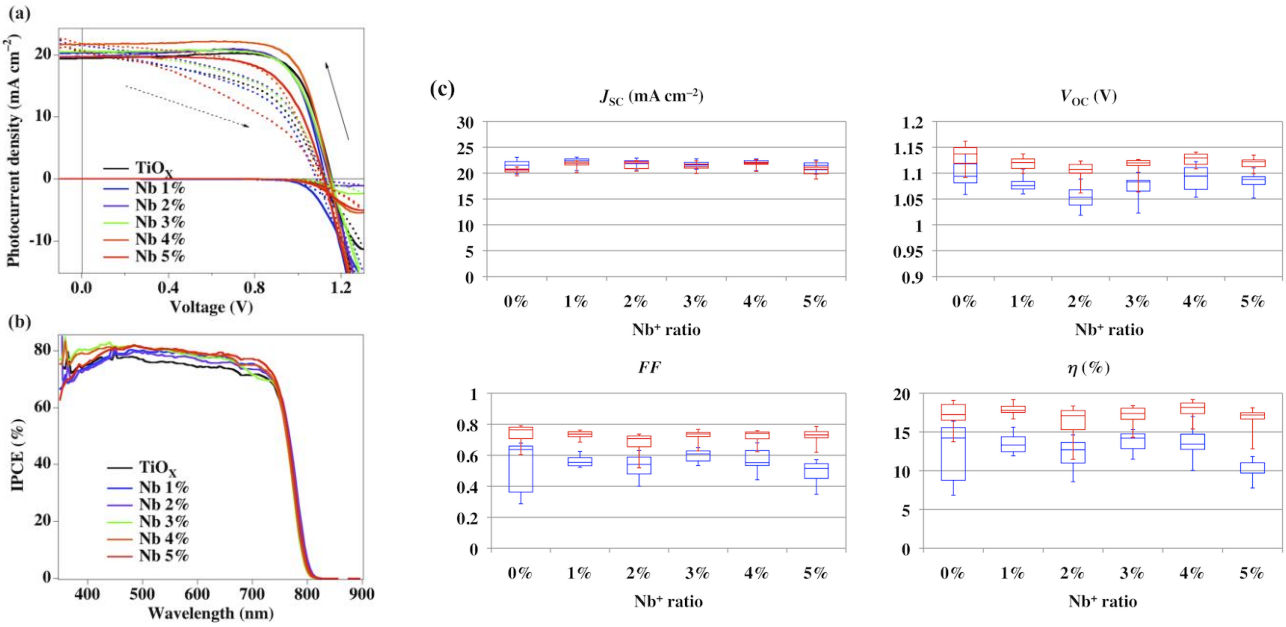

Figure 2. PV data of $(FAPbI_3)_{0.85}(MAPbBr_3)_{0.15}$-based PSCs. (a) J-V curves and (b) IPCE spectra of the typical cells for TiOx and 1~5% Nb-dopded TiO_x CLs.(c) Box plot of the photovoltaic parameters. Blue: forward scan, Red: reverse scan.

Table 2. Photovoltaic parameters of $FA_{0.85}Cs_{0.15}PbI_3$-based PSCs with or w/o different ratio Nb-doped CLs dried at 130 °C.

CL	scan direction[a)]	J_{SC} (mA cm^{-2})	V_{OC} (V)	*FF*	η (%)	*Rs* (Ω)[b)]	No. of cells
TiO_x	forward	22.49±1.03 (23.49)	1.02±0.03 (1.03)	0.37±0.08 (0.55)	8.5±2.2 (13.4)	66±15	20
	reverse	22.94±0.54 (23.87)	1.03±0.06 (1.07)	0.61±0.08 (0.67)	14.5±2.4 (17.0)	35±6	
Nb 4%	forward	23.96±0.27 (24.44)	1.04±0.01 (1.05)	0.64±0.04 (0.69)	15.9±1.3 (17.8)	32±4	11
	reverse	23.91±0.23 (24.22)	1.08±0.01 (1.08)	0.74±0.02 (0.75)	19.0±0.7 (19.8)	20±1	
Nb 5%	forward	23.31±0.81 (22.90)	1.02±0.02 (1.05)	0.49±0.09 (0.65)	11.6±2.3 (15.7)	50±14	17
	reverse	23.38±0.79 (23.23)	1.05±0.02 (1.08)	0.66±0.05 (0.74)	16.3±1.6 (18.6)	30±6	

[a)] Scan direction: forward $J_{SC} \rightarrow V_{OC}$ and reverse: $V_{OC} \rightarrow J_{SC}$. In parentheses, the parameters of the best cell. Cell active area is 5 × 5 mm^2 defined by black mask. [b)] R_s values were calculated from the slope at V_{OC} of *J-V* curves.

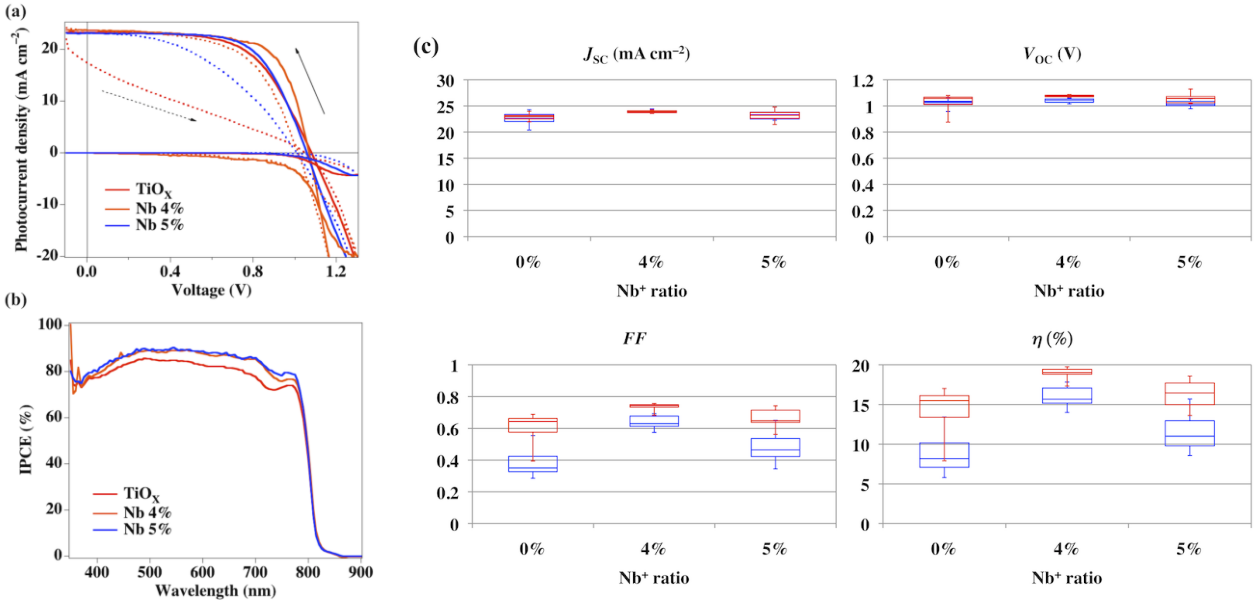

Figure 3. Photovoltaic data of $FA_{0.85}Cs_{0.15}PbI_3$-based PSCs. (a) *J-V* curves and (b) IPCE spectra of the typical cells for non-, 4%, and 5% Nb-doped TiO_x CLs. (c) Box plots of the photovoltaic parameters.

shown in Figure S4). Difference in the transmittance of the CL/FTO substrate is attributed to the thickness of the CL, but independent from drying temperature and Nb doping as shown in Figure 1c and S4. Within UV-vis. spectral region from 350 to 600 nm, thinner CLs presented lower transmittance. This is because the incident light is come from the FTO (CL) side and the light is reflected and scattered at the FTO surface. With increasing the CL thickness, FTO surface texture was flattened, resulting the scattering and reflecting light was reduced. In contrast, longer than 700 nm, transmittance of thick film was decreased with increasing the CL thickness due to the light absorbance.

We attempted to obtain carrier concentration in the Nb/TiO_X films by Hall-effect measurement. However, because of very high sheet resistance of the amorphous TiO_X films, we could not obtain the correct information of carrier density in the TiO_X films (Figure S5).

Photovoltaic properties of mixed perovskite-based PSCs

First, to optimize the Nb/TiO_x CL fabrication process, we employed a $(FAPbI_3)_{0.85}(MAPbBr_3)_{0.15}$ (FA-MA) perovskite as a light absorber material because we have ever developed PSCs based on this material and we can prepare highly efficient photovoltaic device.[73] We used brookite TiO_2 nano-particles as a mesoporous layer, which can provide highly efficient PSCs by low temperature process less than 150 °C.[10,44-47] By changing spin coating speed, we controlled thicknesses of Nb/TiO_x CLs (Figure S6). The thicknesses of the CLs are 40, 70, and 100 nm. Figure S7 shows photocurrent density-voltage (*J-V*) curves and PV data is summarized in Table S1 for FA-MA perovskite-based devices with different thick CLs dried at 150 °C. With decreasing a CL thickness, photocurrent density was significantly improved and short-circuit current density (J_{SC}) of the device based on a 40 nm thick CL reached approximately 21 mA cm^{-2}. V_{OC} values of the three conditions were almost similar ranging from 1.13 to 1.16 V. The best conversion efficiency of 17.3% was achieved on the 40 nm thick CL-based device in reverse scan. It is simply attributed to low resistivity of the thinner CL, resulting higher fill factor (*FF*) and J_{SC} values. Then, we examined influences of dry temperature of the substrate (CL/mesoporous layer) at 100 and 150 °C. For both devices based on the brookite TiO_2 mesoporous films and Nb/TiO_x CLs, *J-V* characteristics in reverse scans ($V_{OC} \rightarrow J_{SC}$) did not present large difference in conversion efficiencies independent on the process temperature. The averaged efficiencies of approximately 16% were achieved. In contrast,

in forward scan of the PSC prepared at 100 °C, the J_{SC} and V_{OC} values were almost similar, but fill factor was significantly deteriorated, resulting hysteretic width increased as shown in Figure S7. For the control TiO_x based device, significantly wide hysteretic behaviours were also observed for both devices prepared at 100 and 150 °C. Compared with PSCs based on a $(FAPbI_3)_{0.85}(MAPbBr_3)_{0.15}$ perovskite and a high temperature sintered TiO_2 CL without Nb-doping, the low-temperature processed devices presented slightly higher conversion efficiency due to high V_{OC} values.[75]

Next, we changed a doping ratio of Nb ion from 1 to 5 mol% in TiO_x CLs, and prepared PSCs using the CLs. Photovoltaic parameters of the PSCs are summarized in Table 1 and Figure 2. The averaged J_{SC} values are ranging a from ca. 20 to 21 mA cm^{-2} and the averaged V_{OC} values of all devices are ranging from 1.05 to 1.16 V. For the (1%) Nb/TiOx CL-based cell, V_{OC} was slightly deteriorated compared with the TiO_x CL-based cell. With increasing Nb-doping ratio, V_{OC} was gradually improved and at the doping ratio of 4%, the V_{OC} reached maximum value, up to 1.15 V, and for 5%-doped cell, V_{OC} was dropped again. For all the devices showed hysteretic *J-V* curves as shown in Figure 2a. The onset wavelength of incident photon-to-current (IPCE) spectra for all cells are well matched at 800 nm (Figure 2b), and integrated photocurrent is ranging from 19 to 21 mA cm^{-2}, matching with J_{SC} values of the *J–V* curves. The hysteresis width was changed depending on Nb-doping ratio (Figure 2c, *FF*). By increasing Nb-doping ratio, extent of hysteresis width was gradually decreased, resulting a *FF* improved in both forward and reverse scans. At the 4% Nb-doping, hysteresis width was minimized. However, adding more Nb ion, (5%) Nb/TiO_X, hysteresis was enhanced again. As a result, the best conversion efficiency was obtained on the 4% Nb-doped TiO_X CL. The best conversion efficiency of 19.1% with J_{SC} of 21.73 mA cm^{-2}, V_{OC} of 1.15 V, and *FF* of 0.76 in the reverse scan was achieved on the cell with aperture area of 5 × 5 mm^2 as shown in Figure 2c. Based on a (4%) Nb/TiOx CL dried at 150 °C, the best conversion efficiency of 19.6% was obtained (in Figure S8 and Table S2). For the 150 °C dried CL-based devices, difference among anneal temperature was decreased compared to the 100 °C dried devices.

Then, we replaced the FA-MA perovskite layer with FA and Cs mixed perovskite: $FA_{0.85}Cs_{0.15}PbI_3$ (FA-Cs) as a highly stable and efficient light absorbing material. Because the best conversion efficiency of a FA-Cs PSC based on high temperature prepared device was achieved on annealing temperature at 130 °C in our preliminary study (see S.I., Figure S9, S10 and Table S3), Nb-doped TiO_x CL and brookite TiO_2 mesoporous layer were dried at 130 °C. A doping ratio of 4% was examined because of the result of FA-MA perovskite, and TiO_x and 5% Nb-doped TiO_x were also used as comparisons. Reflecting the result of FA-MA perovskite, thickness of the CL was less than 40 nm similar with the FA-MA device.

Photovoltaic properties of FA-Cs PSCs based on the TiO_x, 4%, and 5% Nb-doped TiO_x CLs are summarized in Table 2 and Figure 3. Three PSCs showed similar J_{SC} and V_{OC} values independent on Nb-doping ratio. For all devices, J_{SC} values of up to 25 mA cm^{-2} were obtained (Figure 3a), which is higher than that of FA-MA device because of a narrower band gap of FA-Cs perovskite. The IPCE onsets for the FA-Cs PSCs reached approximately 860 nm (Figure 3b). Contrastively, maximum V_{OC} values are approximately 1.05 V, which is slightly lower than that of FA-MA devices. Devices based on a non-doped TiO_x CLs showed awfully large hysteresis and low fill factor due to the high series resistance (R_s), 35±6 Ω in *J-V* curves among the three entries (Figure 3a and c, and Table 2). By 4% Nb-doping, the hysteresis was drastically decreased and R_s was reduced to 20±1 Ω. However, when doping ratio increased to 5%, hysteresis was slightly enhanced similar to the FA-MA devices, and FF decreased attributed to increase of R_s, 30±6 Ω. As a result, the PSC based on the (4%) Nb/TiOx CL showed the best conversion efficiency of 19.8% with J_{SC} of 24.22 mA cm^{-2}, V_{OC} of 1.08 V, and *FF* of 0.75 in the reverse scan, and 17.8% with J_{SC} of 24.44 mA cm^{-2}, V_{OC} of 1.05 V, and *FF* of 0.69 in the forward scan, respectively. The 4% Nb-doped CL showed the highest efficiencies for both FA-MA and FA-Cs perovskite based devices, regarding as independent on type of perovskite. And

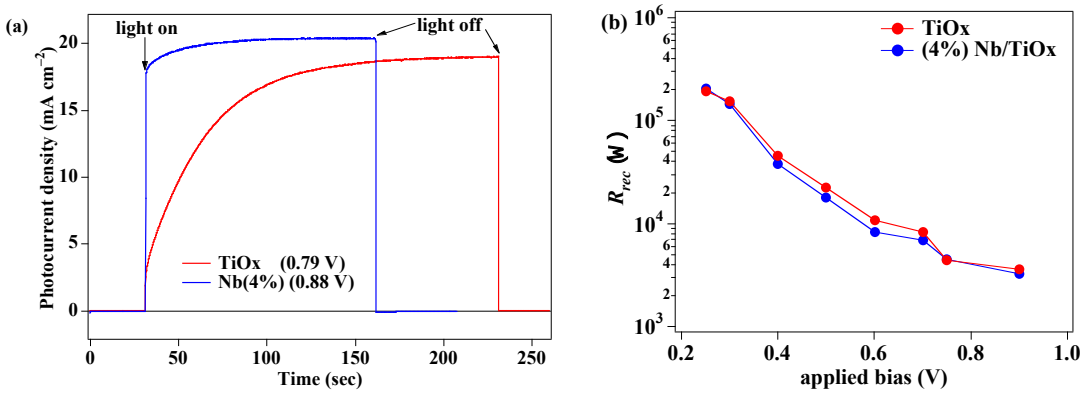

Figure 4. (a) Stady-state photocurrent of FA-Cs PSCs based on TiO_x and (4%) Nb/TiO_x CLs under V_{max} bias. (b) Recombination resistivity (R_{rec}) of FA-Cs PSCs based on TiO_x and (4%) Nb/TiO_x CLs under dark condition with different bias voltages.

the perovskite layers do not almost contact to the CL, because of separation by dense TiO_2 mesoporous layer based on finely small nano-particles (Figure S11); therefore, it is expected that the influence of Nb-doping affected to the interfaces between FTO and TiO_X CL, and/or TiO_X CL and mesoporous layer. Nb alkoxide is more reactive than Ti alokoxyde, therefore, interface among FTO, CL, and mesoporous layers are connected tightly by reactive Nb ions. Over 5% doping, the *R*s value was increased again. It is expected that excess Nb ion distorted the structure of ion positions largely in the TiO_X film.

In order to obtain information about carrier dynamics, we observed steady-state photocurrent density and electrochemical impedance spectroscopy measurement on FA-Cs PSCs based on TiO_X and (4%) Nb/TiO_X CLs. Figure 4a shows time course of steady-state photocurrent density of FA-Cs PSCs based on TiO_X and (4%) Nb/TiO_X CLs measured under 1-sun (AM 1.5G) condition with voltage bias at V_{max}. For the TiO_X based cell, after light on, photocurrent density slowly and gradually increased, and even after 200 sec, photocurrent density reached approximately 18 mA cm^{-2}; however, it is not still saturated and the calculated power out-put of 14.9% was lower compared with the photocurrent density of 21.6 mA cm^{-2} and power out-put of 16.6% obtained from *J-V* measurement. This very slow light response is the origin of the large hysteresis in *J-V* curve. Uchida and Segawa reported that an internal capacitance of PSCs is an origin of *J-V* hysteresis.[73] Previously we confirmed that even a FTO/TiO_2 CL device exhibited *J-V* hysteresis, and concluded that a TiO_2 CL largely contributed to hysteresis behaviors in PSCs.[74] By Nb-doping in a TiO_2, improvement of conductivity, increase in carrier density, and expansion of lattice parameters[68-70,72] are reported, and it is expected that such factors affected to the change in *J-V* hysteresis. In contrast, photocurrent density of the (4%) Nb/TiO_X quickly responded to the light irradiation, and saturated before 100 sec. The photocurrent density exceeds 20 mA cm^{-2} and the out-put power reached 18.0%, which is well matched with those obtained from *J-V* curve, 22.45 mA cm^{-2} and 19.8%, respectively.

Figure 4b shows recombination resistivity (R_{rec}) for FA-Cs PSCs based on TiO_x and (4%) Nb/TiO_x CLs estimated from electrochemical impedance spectroscopy (EIS) measurements under dark condition with different bias voltages. The R_{rec} values of two FA-Cs PSCs do not present significant difference in the blocking property for the carrier recombination. Considering from R_S and R_{rec} of the TiO_X and (4%) Nb/TiO_X CL based devices, the improvement of *FF* by Nb-doping is attributed to the reduction in series resistivity of the CL and/or interfacial resistivity between the brookite TiO_2 mesoporous layer and the CL.

Finally, we examined device durability for a non-encapsulated FA-Cs cell based on the Nb/TiO_x CL by continuous light irradiating steady-state photocurrent measurement under ambient atmosphere; T = 26 °C, RH > 25%. Figure 5 shows *J-V* curves before and after 1 h measurement and steady-state photocurrent with 0.84 V bias voltage, voltage at V_{max}, under 1 sun (AM 1.5G) light irradiation. At first, photocurrent density of 21.0 mA cm^{-2} corresponding to stabilizing efficiency of 17.6% was observed. This efficiency was well matched with the efficiency of 17.7% in *J–V* measurement. After 1 h power generation at P_{max} condition, photocurrent density decreased to 17.6 mA cm^{-2} corresponding to 14.8% of stabilizing efficiency, which retains 85% efficiency of first efficiency. The little difference from the efficiency of 15.7% in *J-V* curve is attributed to change of V_{max}. After the tested sample was stored under dark and dry condition overnight, the conversion efficiency was recovered.

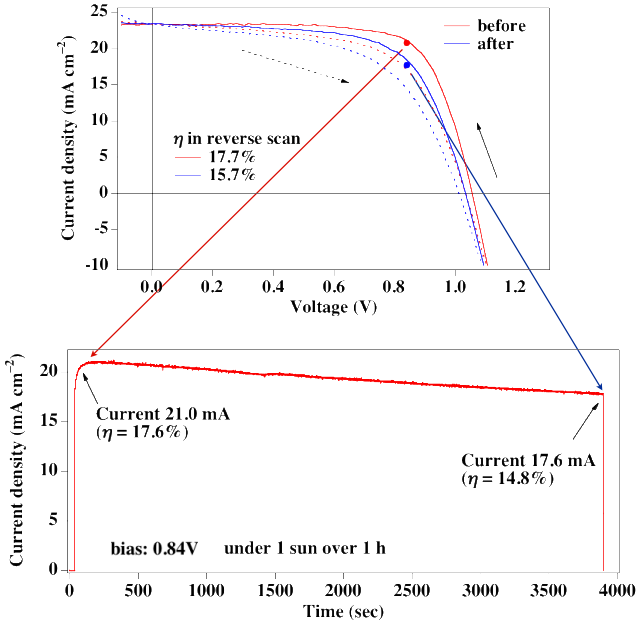

Figure 5. *J-V* curves of FA-Cs based PSC before (red line) and after (blue line) steady-state photocurrent measurement under AM 1.5G 1 sun light condition. The steady-state photocurrent measurement was carried out under ambient condition without any encapsulation.

Conclusions

In conclusion, we successfully developed a simple low-temperature process for highly efficient and durable mesoscopic perovskite solar cells based on a Nb-doped amorphous TiO_x CL and brookite TiO_2 nano-particles, limiting whole process temperature less than annealing temperature of perovskite film. Resistivity of the Nb-doped was decreased with increasing Nb-doping ratio. By XRD and XPS measurements, it is confirmed that the CL is amorphous, and Ti and Nb ions in the CL are +4 and +5 oxidation state, respectively, similar with crystalline metal oxides.

For the PSCs based on FA-MA and FA-Cs perovskites, both PSCs presented the best conversion efficiencies using a 4% Nb-doped TiO_x CL. The PSC based on a 100 °C dried substrate and a $(FAPbI_3)_{0.85}(MAPbBr_3)_{0.15}$ perovskite achieved the best conversion efficiency of 19.1% for 5 × 5 mm^2 aperture area. By replacing the perovskite by $FA_{0.85}Cs_{0.15}PbI_3$ and 130 °C dried substrate, the best efficiency of 19.8% was obtained. The FA-Cs

based cell showed significant device stability. The PSC retained 85% efficiency after 1 h light irradiation by AM 1.5G 1 sun light and 0.84V bias on a non-encapsulated device.

There is still a room for improvement of conversion efficiency, e.g., different metal ion dope, accurate thickness, and preparation temperature optimizations. Such attempt is now undergoing.

Experimental

Materials

All chemicals were purchased from Tokyo Chemical Industry CO., LTD (TCI), Wako Pure Chemical Industries Ltd, and Sigma-Aldrich Japan. All perovskite materials: cesium iodide, ammonium salts (FAI and MABr), and lead halides (PbI_2 and $PbBr_2$) were perovskite grade (TCI). spiro-OMETAD was purchased Sigma-Aldrich. All solvents were super dehydrated grade (Wako). All chemicals were applied to the experiments without further purification. FTO glass substrate and an aqueous suspension of brookite TiO_2 nano-particles (PECC-B01) were obtained from Peccel Technologies, Japan.

Preparation of Peovskite solar cells.

(Nb-doped) TiO_x compact layer and TiO_2 mesoporous layer. Device fabrication was carried out under dry condition (dew point < –20 °C) without any statement. TiO_x and Nb-doped TiO_x (Nb/TiO_x) films were prepared by spin coating method with an EtOH solution of mixture of [Ti(*i*-PrO)$_4$] and [Nb(EtO)$_5$] (100:0 ~ 95:5 / mol%) for 30 sec with arbitrary spin speed. The as-prepared film was dried at 100, 130, and 150 °C for 1h to obtain amorphous Nb/TiO_x CLs.

Then, onto the CL, an ethanolic suspension of brookite TiO_2 nano-particles (18:1, v/v) was spin-coated and dried at same temperature with the scaffold CLs to obtain low-temperature prepared mesoporous substrates under ambient condition.

$(FAPbI_3)_{0.85}(MAPbBr_3)_{0.15}$ perovskite and hole transport layers. A 1.5 M solution of FAI, PbI_2, MABr, and $PbBr_2$ in a mixture of dimethylformamide (DMF) and dimethylsulfoxide (DMSO) (4:1 v/v) was stirred at 70 °C for 1h. The solution was put onto a mesoscopic substrate and spin coated by rotation speed; before spin start, 30 sec kept, 3000 rpm /30 sec, accelerated to 6000 rpm /30 sec during the quick spin, 300 μL of chlorobenzene was casted onto the perovskite film, then, the as-prepared film was a pot-roast vapor-assisted annealed[73] at 100 °C in a petri dish for 15 min, remove the petri dish, and annealed for 5 min. A 7 wt% chlorobenzene solution of 2,2',7,7'-tetrakis(*N*,*N*-di-*p*-methoxyphenylamine)-9,9'-spirobifluorene (*spiro*-OMeTAD) with LiTSFI (0.035 M) in acetonitrile, TBP (0.231 M), and FK209 PF_6 salt (0.002 M) in acetonitrile (in molar ratio, 1 : 0.5 : 3.3 : 0.03) was additives was put on the perovskite by spin coating (3000 rpm for 30 sec), and kept under dry and dark condition overnight. Finally, gold was vacuum evaporated as a counter electrode.

$FA_{0.85}Cs_{0.15}PbI_3$ perovskite and hole transport layers. A 1.2 M solution of FAI, CsI, and PbI_2 in a mixture of dimethylformamide (DMF) and dimethylsulfoxide (DMSO) (4:1 v/v) was stirred at 70 °C for 1h. The solution was put onto a mesoscopic substrate and spin coated by rotation speed; before spin start, 30 sec kept, 3000 rpm /30 sec, accelerated to 6000 rpm /30 sec during the quick spin, 300 μL of chlorobenzene was casted onto the perovskite film, then, the as-prepared film was vapor-assisted annealed at 130 °C in a petri dish for 10 min, remove the petri dish, and annealed for 5 min. A chlorobenzene solution of *spiro*-OMeTAD with the additives was put on the perovskite and gold was vacuum evaporated as a counter electrode.

Measurements

SEM and XRD measurements. SEM measurements were performed by SU8000 (Hitachi High-Technologies Co.) XRD patterns were measured by D8 DISCOVER (Bruker-AXS K. K.) with Cu Kα radiation under operation condition of 40kV, 40mA.

Resistivity measurements. A CL casted on a FTO substrate similar with the PSC was prepared. On the CL, Au was vacuum deposited as an electrode. The sample structures are presented in Figure 2a for ITO/thin CL and S3 for FTO/thick CL, respectively. *I-V* measurement was carried out similar condition of the PSC device (see below).

Photovoltaic measurements. Cell active area (5 × 5 mm^2) was defined by a black metal mask. Photocurrent density-voltage (*J-V*) curves were recorded using with PEC-L01 solar simulator (Peccell Technologies) under AM1.5G condition (100 mW cm^{-2}). Measurement condition; Step voltage: 0.01 V, search delay: 0.05 sec, and hold time: 0.1 sec. Incident photon-to-current conversion efficiency (IPCE) spectra were observed by PEC-S20 spectrometer (Peccell Technologies).

XPS measurements. XPS spectra were measured using an AXIS Nova (Kratos Analytical Ltd) equipped with a monochromatic Al K X-ray source (150 W), and the pass-energy of the spectrometer was set to 160 or 40 eV for the survey or core spectrum measurement, respectively.

Electrochemical impedance spectroscopy (EIS) measurement. EIS measurements were performed using an SI 1287 ELECTROCHEMICAL INTERFACE and SI 1260 IMPEDANCE/GAIN-PHASE ANALYZER (Toyo Technica). The measurements were carried out under dark condition with different bias voltages. R_{rec} values were calculated from the obtained Nyquist plot data by curve fitting using a Z-plot software.

Hall-effect measurements. Hall-effect measurement was carried out using a self-made system consisting of 0.5 T permanent magnet, keithley 6220 DC Current Source, 2182A nanovoltmeter and 7001 switching system with 7065 Hall Effect Card. The TiO_X samples were prepared on a glass substrate. TiO_X film thickness was approximately 7 nm and the sample size was 1.25 × 1.25 cm^2. Electrodes were contacted at each corner and measured between diagonal corners.

Acknowledgements

This research was supported by Advanced Low Carbon Technology Research and Development Program (ALCA) by Japan Science and Technology Agent (JST) and Grant-in-Aid for Scientific Research C (17K05968) of Japanese Society for Promotion of Science (JSPS). We would like to appreciate supports for SEM, XRD, and EIS measurements by Professor Hiroshi Segawa (RCAST, The University of Tokyo).

Notes and references

1 A. Kojima, K. Teshima, Y. Shirai and T. Miyasaka, *J. Am. Chem. Soc*., 2009, **131**, 6050–6051.
2 M. M. Lee, J. Teuscher, T. Miyasaka, T. N. Murakami and H. J. Snaith, *Science*, 2012, **338**, 643–647.
3 H.-S. Kim, C.-R. Lee, J.-H. Im, K.-B. Lee, T. Moehl, A. Marchioro, S.-J. Moon, R. Humphry-Baker, J.-H. Yum, J. E. Moser, M. Grätzel and N.-G. Park, *Sci. Rep*., 2012, **2**, 591.
4 N.-G. Park, M. Grätzel, T. Miyasaka, K. Zhu and K. Emery, *Nat. Ener*. 2016, **1**, 16152.
5 M. Cai, Y. Wu, H. Chen, X. Yang, Y. Qiang and L. Han, *Adv. Sci*., 2017, **4**, 1600269.
6 Research Cell Efficiency Records. NREL, http://www.nrel.gov/ncpv/, accessed February 2018.
7 D. Yang, R. Yang, J. Zhang, Z. Yang, S. (F.) Liu and C. Li, *Energy Environ. Sci*., 2015, **8**, 3208-3214.
8 D. Yang, R. Yang, X. Ren, X. Zhu, Z. Yang, C. Li and S. (F.) Liu, *Adv. Mater*., 2016, **28**, 5206-5213.
9 J. Feng, Z. Yang, D. Yang, X. Ren, X. Zhu, Z. Jin, W. Zi, Q. Wei, and S. (F.) Liu, *Nano Energy*, 2017, **36**, 1-8.
10 A. Kogo, M. Ikegami and T. Miyasaka, *Chem. Commun*., 2016, **52**, 8119.
11 S.-Y. Lin, T.-S. Su, T.-Y. Hsieh, P.-C. Lo and T.-C. Wei, *Adv. Energy Mater*., 2017, **7**, 1700169.
12 Y. Zhang, Z. Wu, P. Li, L. K. Ono, Y. Qi, J. Zhou, H. Shen, C. Surya and Z. Zheng, *Adv. Energy Mater*., 2018, **8**, 1701569.
13 Z. Zhou, X. Li, M. Cai, F. Xie, Y. Wu, Z. Lan, X. Yang, Y. Qiang, A. Islam and L. Han, *Adv. Energy Mater*., 2017, **7**, 1700763.
14 A. H. Slavney, L. Leppert, D. Bartesaghi, A. Gold-Parker, M. F. Toney, T. J. Savenije, J. B. Neaton and H. I. Karunadasa, *J. Am. Chem. Soc*., 2017, **139**, 5015-5018.
15 B.-W. Park, B. Philippe, X. Zhang, H. Rensmo, G. Boschloo and E. M. J. Johansson, *Adv. Mater*., 2015, **27**, 6806-6813.
16 X.-G. Zhao, J.-H. Yang, Y. Fu, D. Yang, Q. Xu, L. Yu, S.-H. Wei and L. Zhang, *J. Am. Chem. Soc*., 2017, **139**. 2630-2638.
17 Y. Kim, Z. Yang, A. Jain, O. Voznyy, G.-H. Kim, M. Liu, L. N. Quan, F. P. G. de Arquer, R. Comin, J. Z. Fan and E. H. Sargent, *Angew. Chem. Int. Ed*., 2016, **55**, 9586-9590.
18 R. L. Z. Hoye, L. C. Lee, R. C. Kurchin, T. N. Huq, K. H. L. Zhang, M. Sponseller, L. Nienhaus, R. E. Brandt, J. Jean, J. A. Polizzotti, A. Kursumović, M. G. Bawendi, V. Bulović, V. Stevanović, T. Buonassisi and J. L. MacManus-Driscoll, *Adv. Mater*., 2017, **29**, 1702176.
19 S. A. Adonin, L. A. Frolova, M. N. Sokolov, G. V. Shilov, D. V. Korchagin, V. P. Fedin, S. M. Aldoshin, K. J. Stevenson and P. A. Troshin, *Adv. Energy Mater*., 2017, DOI: 10.1002/aenm.201701140.
20 R. Nie, H.-S. Yun, M.-J. Paik, A. Mehta, B.-W. Park, Y. C. Choi and S. I. Seok, Adv. Energy Mater., 2017, DOI: 10.1002/aenm.201701901.
21 H. Uzu, M. Ichikawa, M. Hino, K. Nakano, T. Meguro, J. L. Hernandez, H.-S. Kim, N.-G. Park and K. Yamamoto, *Appl. Phys. Lett*., 2015, **106**, 013506.
22 J. P. Mailoa, C. D. Bailie, E. C. Johlin, E. T. Hoke, A. J. Akey, W. H. Nguyen, M. D. McGehee and T. Buonassisi, *Appl. Phys. Lett*., 2015, **106**, 121105.
23 F. Lang, M. A. Gluba, S. Albrecht, J. Rappich, L. Korte, B. Rech and N. H. Nickel, *J. Phys. Chem. Lett*., 2015, **6**, 2745-2750.
24 J. Werner, C.-H. Weng, A. Walter, L. Fesquet, J. P. Seif, S. De Wolf, B. Niesen and C. Ballif, *J. Phys. Chem. Lett*., 2016, **7**, 161-166.
25 P. Löper, S.-J. Moon, S. M. de Nicolas, B. Niesen, M. Ledinsky, S. Nicolay, J. Bailat, J.-H. Yum, S. De Wolfa and C. Ballif, *Phys. Chem. Chem. Phys*., 2015, **17**, 1619-1629.
26 S. Albrecht, M. Saliba, J. P. C. Baena, F. Lang, L. Kegelmann, M. Mews, L. Steier, A. Abate, J. Rappich, L. Korte, R. Schlatmann, M. K. Nazeeruddin, A. Hagfeldt, M. Grätzel and B. Rech, *Energy Environ. Sci*., 2016, **9**, 81-88.
27 I. Almansouri, A. Ho-Baillie and M. A. Green, *Jpn. J. Appl. Phys.*, 2015, **54**, 08KD04.
28 D. P. McMeekin, G. Sadoughi, W. Rehman, G. E. Eperon, M. Saliba, M. T. Hörantner, A. Haghighirad, N. Sakai, L. Korte, B. Rech, M. B. Johnston, L. M. Herz, H. J. Snaith, *Science*, 2016, **351**, 151-155.
29 K. A. Bush, A. F. Palmstrom, Z. J. Yu, M. Boccard, R. Cheacharoen, J. P. Mailoa, D. P. McMeekin, R. L. Z. Hoye, C. D. Bailie, T. Leijtens, I. M. Peters, M. C. Minichetti, N. Rolston, R. Prasanna, S. Sofia, D. Harwood, W. Ma, F. Moghadam, H. J. Snaith, T. Buonassisi, Z. C. Holman, S. F. Bent and M. D. McGehee, *Nat. Ener*., 2017, **2**, 17009.
30 L. Kranz, A. Abate, T. Feurer, F. Fu, E. Avancini, J. Löckinger, P. Reinhard, S. M. Zakeeruddin, M. Grätzel, S. Buecheler and A. N. Tiwari, *J. Phys. Chem. Lett*., 2015, **6**, 2676-2681.
31 Y. (M.) Yang, Q. Chen, Y.-T. Hsieh, T.-B. Song, Ni. De Marco, H. Zhou and Y. Yang, *ACS Nano*, 2015, **9**, 7714-7721.
32 T. Todorov, T. Gershon, O. Gunawan, Y. S. Lee, C. Sturdevant, L.-Y. Chang and S. Guha, *Adv. Energy Mater*., 2015, **9**, 1500799.
33 C. D. Bailie, M. G. Christoforo, J. P. Mailoa, A. R. Bowring, E. L. Unger, W. H. Nguyen, J. Burschka, N. Pellet, J. Z. Lee, M. Grätzel, R. Noufi, T. Buonassisi, A. Salleo and M. D. McGehee, *Energy Environ. Sci*., 2015, **8**, 956-963.
34 F. Fu, T. Feurer, T. P. Weiss, S. Pisoni, E. Avancini, C. Andres, S. Buecheler and A. N. Tiwari, *Nat. Ener*., 2016, **2**, 16190.
35 A. Guchhait, H. A. Dewi, S. W. Leow, H. Wang, G. Han, F. B. Suhaimi, S. Mhaisalkar, L. H. Wong and N. Mathews, *ACS Energy Lett*., 2017, **2**, 807-812.
36 P. Mantilla-Perez, T. Feurer, J.-P. Correa-Baena, Q. Liu, S. Colodrero, J. Toudert, M. Saliba, S. Buecheler, A. Hagfeldt, A. N. Tiwari and J. Martorell, *ACS Photonics*, 2017, **4**, 861-867.
37 H. Shen, T. Duong, J. Peng, D. Jacobs, N. Wu, J. Gong, Y. Wu, S. K. Karuturi, X. Fu, K. Weber, X. Xiao, T. P. White and K. Catchpole, *Energy Environ. Sci*., 2017, DOI: 10.1039/c7ee02627g.
38 T. Todorov, T. Gershon, O. Gunawan, C. Sturdevant and S. Guha, *Appl. Phys. Lett*., 2014, **105**, 173902.
39 J. H. Heo and S. H. Im, *Adv. Mater*., 2015, **28**, 5121-5125.
40 F. Jiang, T. Liu, B. Luo, J. Tong, F. Qin, S. Xiong, Z. Li and Y. Zhou, *J. Mater. Chem. A*, 2016, **4**, 1208-1213.
41 D. Forgács, L. Gil-Escrig, D. Pérez-Del-Rey, C. Momblona, J. Werner, B. Niesen, C. Ballif, M. Sessolo and H. J. Bolink, *Adv. Energy Mater*., 2017, **7**, 1602121.
42 D. P. McMeekin, G. Sadoughi, W. Rehman, G. E. Eperon, M. Saliba, M. T. Hörantner, A. Haghighirad, N. Sakai, L. Korte, B. Rech, M. B. Johnston, L. M. Herz, H. J. Snaith, *Science*, 2016, **351**, 151-155.
43 D. Zhao, Y. Yu, C. Wang, W. Liao, N. Shrestha, C. R. Grice, A. J. Cimaroli, L. Guan, R. J. Ellingson, K. Zhu, X. Zhao, R.-G. Xiong and Y. Yan, *Nat. Ener*., 2017, **2**, 17018.
44 A. Kogo, Y. Sanehira, M. Ikegami and T. Miyasaka, *Chem. Lett*., 2016, **45**, 143.

45 A. Kogo, Y. Sanehira, M. Ikegami and T. Miyasaka, *J. Mater. Chem. A,* 2015, **3**, 20952.
46 A. Kogo, S. Iwasaki, M. Ikegami and T. Miyasaka, *Chem. Lett*., 2017, **46**, 530-532.
47 A. Kogo, Y. Sanehira, Y. Numata, M. IKegami and T. Miyasaka, *ACS Appl. Mater. Interfaces*, 2018, **10**, 2224-2229.
48 K. Sato, S. Kim, S. Komuro and X. Zhao, *Jpn. J. Appl. Phys*., 2016, **55**, 06GJ10.
49 J.-H. Bae, J.-M. Moon, J.-W. Kang, H.-D. Park, J.-J. Kim, W. J. Choc and H.-K. Kima, *J. Electrochem. Soc*., 2007, **154**, J81-J85.
50 M. A. Mahmud, N. K. Elumalai, M. B. Upama, D. Wang, A. M. Soufiani, M. Wright, C. Xu, F. Haque and A. Uddin, *ACS Appl. Mater. Interfaces*, 2017, **9**, 33841-33854.
51 J. H. Heo, M. S. You, M. H. Chang, W. Yin, T. K. Ahn, S.-J. Lee, S.-J. Sung, D. H. Kim, S. H. Im, *Nano Energy*, 2015, **15**, 530-539.
52 F. Giordano, A. Abate, J. P. C. Baena, M. Saliba, T. Matsui, S. H. Im, S. M. Zakeeruddin, M. K. Nazeeruddin, A. Hagfeldt and M. Graetzel, *Nat. Commun*. 2016, **7**, 10379.
53 M.-C. Wu, S.-H. Chan, M.-H. Jao, W.-F. Su, *Sol. Energy Mater. Sol. Cells*, 2016, **157**, 447-453.
54 H. Zhou, Q. Chen, G. Li, S. Luo, T. Song, H. Duan, Z. Hong, J. You, Y. Liu and Y. Yang, *Science*, 2014, **345**, 6196.
55 X. Yin, Y. Guo, Z. Xue, P. Xu, M. He and B. Liu, *Nano Res*., 2015, **8**, 1997-2003.
56 G. Yin, J. Ma, H. Jiang, J. Li, D. Yang, F. Gao, J. Zeng, Z. Liu and S. F. Liu, *ACS Appl. Mater. Interfaces*, 2017, **9**, 10752-10758.
57 B.-X. Chen, H.-S. Rao, W.-G. Li, Y.-F. Xu, H.-Y. Chen, D.-B. Kuang and C.-Y. Su, *J. Mater. Chem. A*, 2016, **4**, 5647-5653.
58 W. Chen, Y. Wu, Y. Yue, J. Liu, W. Zhang, X. Yang, H. Chen, E. Bi, A. Islam, M. Gratzel, L. Han, *Science*, 2015, **350**, 944-948.
59 X. Li, J. Yang, Q. Jiang, W. Chu, D. Zhang, Z. Zhou and J. Xin, *ACS Appl. Mater. Interfaces*, 2017, **9**, 41354-41362.
60 T. Singh, S. Öz, A. Sasinska, R. Frohnhoven, S. Mathur and T. Miyasaka, *Adv. Func. Mater*., 2018, DOI: 10.1002/adfm.201706287.
61 Y. Xiang, Z. Ma, J. Zhuang, H. Lu, C. Jia, J. Luo, H. Li and X. Cheng, *J. Phys. Chem. C*, 2017, **121**, 20150-20157.
62 M. Park, J.-Y. Kim, H. J. Son, C.-H. Lee, S. S. Jang and M. J. Ko, *Nano Energy*, 2016, **26**, 208-215.
63 X. Ren, D. Yang, Z. Yang, J. Feng, X. Zhu, J. Niu, Y. Liu, W. Zhao and S. F. Liu, *ACS Appl. Mater. Interfaces*, 2017, **9**, 2421-2429.
64 G. Yang, H. Lei, H. Tao, X. Zheng, J. Ma, Q. Liu, W. Ke, Z. Chen, L. Xi, P. Qin, Z. Chen, M. Qin, X. Lu, Y. Yan, G. Fang, *Small*, 2017, **13**, 1601769.
65 S. S. Shin, E. J. Yeom, W. S. Yang, S. Hur, M. G. Kim, J. Im, J. Seo, J. H. Noh and S. I. Seok, *Science*, 2017, **356**, 167-171.
66 G. Li, Y. Jiang, S. Deng, A. Tam, P. Xu, M. Wong and H.-S. Kwok, *Adv. Sci*., 2017, **4**, 1700463.
67 W. Chen, F.-Z. Liu, X.-Y. Feng, A. B. Djurišić , W. K. Chan and Z.-B. He, *Adv. Energy Mater*., 2017, **7**, 1700722.
68 Y. Furubayashi, T. Hitosugi, Y. Yamamoto, K. Inaba, G. Kinoda, Y. Hirose, T. Shimada and T. Hasegawa, *Appl. Phys. Lett*., 2005, **86**, 252101.
69 T. Hitosugi, Y. Furubayashi, A. Ueda, K. Itabashi, K. Inaba, Y. Hirose, G. Kinoda, Y. Yamamoto, T. Shimada and T. Hasegawa, *Jpn. J. Appl. Phys.*, 2005, **44**, L1063.
70 Y. Furubayashi, T. Hitosugi, and T. Hasegawa, *Appl. Phys. Lett*., 2006, **88**, 226103.
71 R. D. Shannon, Acta Crystallogr. A, 1976, **32**, 751.
72 G. Sahasrabudhe, J. Krizan, S. L. Bergman, R. J. Cava and J. Schwartz, *Chem. Mater*., 2016, **28**, 3639-3633.
73 L. Cojocaru, S. Uchida, K. Tamaki, P. V. V. Jayaweera, S. Kaneko, J. Nakazaki, T. Kubo and H. Segawa, *Sci. Rep*., 2017, **7**, 11790.
74 A. K. Jena, H.-W. Chen, A. Kogo, Y. Sanehira, M. Ikegami and T. Miyasaka, *ACS Appl. Mater. Interfaces*, 2015, **7**, 9817–9823.
75 Y. Numata, A. Kogo, A. Udagawa, H. Kunugita, K. Ema, Y. Sanehira and T. Miyasaka, *ACS Appl. Mater. Interfaces*, 2017, **9**, 18739-18747.

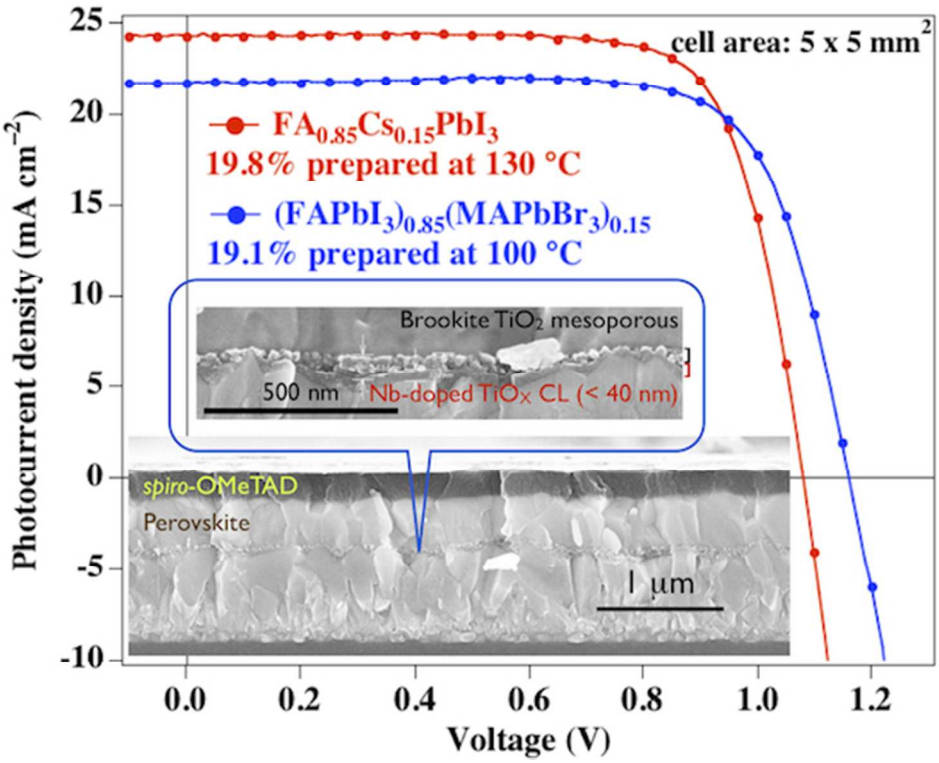

109x84mm (150 x 150 DPI)